Lab on a Chip

Machine learning-aided quantification of antibody-based cancer immunotherapy by Natural Killer cells in microfluidic droplets

Journal:	*Lab on a Chip*
Manuscript ID	LC-ART-02-2020-000158.R1
Article Type:	Paper
Date Submitted by the Author:	25-Apr-2020
Complete List of Authors:	Sarkar, Saheli; Northeastern University Kang, Wenjing; Northeastern University, Pharmaceutical Sciences Jiang, Songyao; Northeastern University Li, Kunpeng; Northeastern University Ray, Somak; Northeastern University Luther, Ed; Northeastern University, Pharmaceutical Sciences Ivanov, Alexander ; Northeastern University Fu, Yun; Northeastern University Konry, Tania; Northeastern University; Harvard University

ARTICLE

Machine learning-aided quantification of antibody-based cancer immunotherapy by Natural Killer cells in microfluidic droplets

Received 00th January 20xx,
Accepted 00th January 20xx

DOI: 10.1039/x0xx00000x

Saheli Sarkar[a], Wenjing Kang[a], Songyao Jiang[b], Kunpeng Li[b], Somak Ray[c], Ed Luther[a], Alexander R. Ivanov[c], Yun Fu[b,d], Tania Konry[a†]

Natural Killer (NK) cells have emerged as an effective alternative option to T cell-based immunotherapies, particularly against liquid (hematologic) tumors. However, the effectiveness of NK cell therapy has been less than optimal for solid tumors, partly due to the heterogeneity in target interaction leading to variable anti-tumor cytotoxicity. This paper describes a microfluidic droplet-based cytotoxicity assay for quantitative comparison of immunotherapeutic NK-92 cell interaction with various types of target cells. Machine learning algorithms were developed to assess the dynamics of individual effector-target cell pair conjugation and target death in droplets in a semi-automated manner. Our results showed that while short contacts were sufficient to induce potent killing of hematological cancer cells, long-lasting stable conjugation with NK-92 cells were unable to kill HER2$^+$ solid tumor cells (SKOV3, SKBR3) significantly. NK-92 cells that were engineered to express FcγRIII (CD16) mediated antibody-dependent cellular cytotoxicity (ADCC) selectively against HER2$^+$ cells upon addition of Herceptin (trastuzumab). The requirement of CD16, Herceptin and specific pre-incubation temperature served as three inputs to generate a molecular logic function with HER2$^+$ cell death as the output. Mass proteomic analysis of the two effector cell lines suggested differential changes in adhesion, exocytosis, metabolism, transport and activation of upstream regulators and cytotoxicity mediators, which can be utilized to regulate specific functionalities of NK-92 cells in future. These results suggest that this semi-automated single cell assay can reveal the variability and functional potency of NK cells and may be used to optimize immunotherapeutic efficacy for preclinical analyses.

Introduction

High affinity T cell receptor and chimeric antigen receptor (CAR)- modified T cells have proved to be an exciting therapeutic means in battling cancer, recently gaining Food and Drug Administration (FDA) approval for the treatment of specific types of hematologic malignancies. There are, however, significant challenges associated with CAR-T immunotherapy, such as off-target cytokine release, systemic toxicity and unregulated killing of healthy cells [1]. Existing anticancer immunotherapies have also met with limited success in treatment of solid tumors due to low tumor selectivity and poor therapeutic potency. Furthermore, the cost of personalized adoptive T cell therapy can be prohibitive for many patients[2].

Other cell-based immunotherapies, such as Natural Killer (NK) cells, have become promising alternative resources as they not only express strong cytotoxic potential via natural cytotoxicity receptors (NCRs) but also kill target cells by antibody-dependent cell-mediated cytotoxicity (ADCC). NK cells persist in host systems for shorter time periods compared to T cells [3]. NK cell lines such as NK-92 have been tested against different cancer types in phase I clinical trials [4]. The NK-92 line is also amenable to genetic engineering and has been transfected with high affinity CD16 allele for mediating ADCC [5]. Pre-clinical and phase I clinical trials with this line have shown encouraging results [3, 6]. However, while NK-92 cells exhibit high levels of anti-tumor cytotoxicity against hematologic malignancies, their response to solid tumor cells such as HER2 (human epidermal growth factor receptor 2)-positive cancers in breast and ovary are still being characterized [3, 6].

Like primary NK cells, NK-92 cells form immunological synapses with their targets and release lytic granules loaded with cytotoxic components [7]. Longitudinal analysis of cellular dynamics using microscale platforms such as microwells and droplets has shown that the interactions between effector lymphocytes and target cells are heterogeneous at single cell level [8, 9, 10]. The variability in conjugation timings, stability of contact, migration patterns and cytolysis may extend to mechanisms of actions related to ADCC, as observed in in vivo studies [11]. CD16 receptor polymorphism and receptor shedding

[a.] *Department of Pharmaceutical Sciences, Northeastern University, 360 Huntington Avenue, Boston, MA, USA.*
[b.] *Department of Electrical and Computer Engineering, College of Engineering, and College of Computer and Information Science, Northeastern University, 360 Huntington Avenue, Boston, MA, USA.*
[c.] *Barnett Institute of Chemical and Biological Analysis, Department of Chemistry and Chemical Biology, Northeastern University, Northeastern University, 360 Huntington Avenue, Boston, MA, USA.*
[d.] *Department of Electrical and Computer Engineering, College of Engineering, and Khoury College of Computer Science, Northeastern University, 360 Huntington Avenue, Boston, MA, USA.*
† Corresponding author email: t.konry@neu.edu.
Electronic Supplementary Information (ESI) available: [details of any supplementary information available should be included here]. See DOI: 10.1039/x0xx00000x

can also affect the cytotoxic efficiency of CD16$^+$ cells [12]. Some studies with CD16$^+$ NK-92 have employed high effector (E)-target (T) cell ratios and prolonged (18 hrs) exposure to kill cancer lines *in vitro* [5,13]. Whether this is due to an inability of the NK cells to seek out and establish contacts rapidly at low E:T, or the inability to maintain persistent contact required for killing, is not clear. The standard assays such as ^{51}Chromium release and flow cytometry-based assays that measure functional cytotoxicity of effector lymphocytes cannot resolve these questions as they do not track specific cellular conjugates over time. The introduction of a transgene can also have indirect consequences at transcriptomic and phenotypic level, causing off-target differences to biochemical processes [14]. No study has investigated the possible modifications of the proteome of engineered NK cells, together with the dynamic single cell analysis of functional heterogeneity. This approach could provide insight into the killing strategies of NK cell-based immunotherapies, which can then be optimized by the addition of specific drugs or further genetic manipulation.

One of the main drawbacks of high throughput time-lapse microscopic studies is the size and complexity of the acquired datasets, which has been addressed by the development of automated image analysis programs. Typically, image analysis workflows involve cell segmentation based on morphological markers (e.g., size, shape, subcellular organelles), feature extraction and classification of identity [15]. An efficient segmentation approach relies on clear detection of cell outlines and edges, thereby requiring frequent auto-focusing during long-term imaging or multidimensional imaging (e.g., z-stacks) per time frame [16]. The problem becomes more complicated when multiple cell types and organoids are present, necessitating advanced segmentation methods such as one using Markov Random Fields (MRFs) [17]. Recently, machine learning strategies have been applied to solve some of the limitations in conventional image analysis pipelines [16]. Supervised machine learning methods such as deep learning have consistently outperformed other analytical approaches and enabled resolution of different phenotypes including *E. coli*, *S. cerevisiae* and mammalian cells [18]. Most studies focus on identifying individual cells from morphological features (size, orientation, lamellipodia, vesicles), fluorescently labelled organelles and proteins [18-21]. Here, we have developed a deep learning algorithm to measure the dynamic profile of live E-T cell interactions at 1:1 ratio. The algorithm is designed to identify cells confined within picoliter-volume microfluidic droplets, which allows the cells to be mobile and form short-lived synapses that are characteristic of many immune cell interactions [22, 23]. This semi-automated analytical method depicted high accuracy in quantifying interactive parameters including conjugation duration, frequency and cell death.

We implemented the droplet microfluidics-based cytotoxicity imaging approach to investigate NK-92 cell-mediated cytolysis of blood and HER2$^+$ solid tumor cells. The results indicate that parental NK-92 cell conjugation with blood cancer cells (K562, DOHH2) led to efficient killing, but not in the case of HER2-overexpressing cancer cells of different origins. CD16$^+$ modified NK-92 lines caused death selectively following incubation of anti-HER2 drug Herceptin. In essence, the combinatorial treatment acted as "AND" logic gate and promoted tumor targeting. We also determined that overexpression of CD16$^+$ had altered the abundance levels of a subset of proteins associated with key biological processes in the modified line compared to the parental cell line. Overall, this study provides an effective technique for measuring NK-92 cell dynamics, functional efficacy and heterogeneity at single cell resolution.

Experimental

Cell lines and culture

The parental NK-92 cells and the NK-92 cells expressing high affinity variant (V158) of the CD16 FcγRIII were developed and generously provided by Nantkwest Inc (Woburn, MA) [5, 13, 24]. All NK-92 cell lines were cultured in phenol free XVivo-10 medium (Lonza, Walkersville, MD) supplemented with 5% heat-inactivated human AB serum (Fisher Scientific, Waltham, MA). The parental NK-92 media was also supplemented with 500 IU/mL recombinant human IL-2 (ProSpec Bio, Israel).

Human tumor cell lines (K562: chronic myelogenous leukemia, DOHH2: B cell lymphoma; SKOV3: ovarian carcinoma, SKBR3: breast carcinoma) were obtained from American Type Culture Collection (ATCC, Manassas, VA). The target cells were maintained in RPMI-1640 medium supplemented with 1X L-Glutamine, 10% Fetal Bovine Serum (FBS) and 1% Antibiotic-Antimycotic solution (Corning Cellgro, Manassas, VA). All cells were grown at 37°C and 5% CO_2 in a humidified atmosphere. Cancer cell lines were routinely passaged every three days and harvested at a density of 1×10^6 viable cells/mL. NK-92 cell lines were seeded at densities of 0.5×10^6 cells/mL.

Microfluidic device fabrication and droplet generation

Sub-nanoliter volume droplets were formed, containing unabeled effector and fluorescently labeled target cells at the flow focusing junction of an integrated droplet generation and docking device. The design and fabrication of this device has been described previously [8, 9, 25, 26]. More details are available in Supplementary Methods.

Antibody treatment and ADCC assay in droplets

Herceptin stocks (20mg/mL) were provided by Nantkwest Inc and stored at 4^{o}C. Target cancer cells, labeled with Calcein AM, were pre-treated with Herceptin (1µg/ml)-supplemented RPMI-1640 growth media at room temperature (RT) or 37^{o}C [5]. The duration of pre-treatment varied from 30 to 60 min. Herceptin was freshly diluted in RPMI-1640 media from stock solutions prior to incubation. The antibody-cell conjugates were loaded in syringes immediately afterwards for encapsulation in droplets. Viability of target cells was assessed by the presence of Calcein AM fluorescence (See Supplementary Methods).

Preparation of cell lysate, digestion and LC/MS/MS

Cell pellets were resuspended in 8M urea, 2M thiourea, 5mM DTT in 0.1M ammonium bicarbonate pH 8. The suspension was vortexed for 2 min and sonicated for 5 min, spun down and incubated for 30 min at room temperature. Iodoacetamide was added to 10mM and

further incubated for 30 min at room temperature in the dark. Suspension was centrifuged at 15,000 rpm and supernatant transferred to a new tube. Protein concentration was measured by Qubit (Thermo Fisher Scientific). 10 µg of protein was digested first with 1 µg of LysC (in 50 µL of solution) for 4hrs at 37°C after which 50 µl of water was added to the solution with 1µg of trypsin and incubated overnight at 37°C. Samples were dried down and resuspended in 2% formic acid. 1 µg of the resulting digest was analyzed for each sample. The sample was loaded with the autosampler directly onto a self-packed column, which was made from a 75 µm ID, 360 µm OD capillary filled with 25cm of 1.9µm Reprosil-Pur C18 AQ. Peptides were eluted at 200 nL/min from the column using a Dionex 3000 HPLC with a 115 min gradient from 5% buffer B to 20% buffer B (100 % acetonitrile, 0.1% formic acid). The gradient was switched from 20% to 80% buffer B over 2 min and held constant for 3 min. Finally, the gradient was changed from 80% buffer B to 99% buffer A (100% water, 0.1% formic acid) over 1 min, and then held constant at 99% buffer A for 15 minutes. The application of a 2.5 kV distal voltage electrosprayed the eluting peptides directly into the Thermo Orbitrap Fusion mass spectrometer equipped with a Flex Source (Thermo Scientific). Mass spectrometer-scanning functions and HPLC gradients were controlled by the Xcalibur software (Thermo Scientific). The mass spectrometer was set to scan MS1 at 120,000 resolution with an AGC target set at 4e5. The scan range was m/z 375-1500. For MS2, spectra were acquired in the ion trap with an AGC target of 3e4 and a maximum IT at 35 ms. The top peaks were analyzed by MS2 for a cycle time of 3 sec. Peptides were isolated with an isolation window of m/z 1.6 and fragmented at 28 CE. Only ions with a charge state of 2 through 7 were considered for MS2. Dynamic exclusion was set at 30 sec.

Data and bioinformatics analysis

Mass spectrometry data were analyzed with ProteomeDiscoverer 2.3 and searched against a human protein database (UniProt, released March 13, 2018) containing common contaminant proteins. Protein quantitation was performed through LFQ analysis using ProteomeDiscoverer v. 2.3. The FDR ≤ 1% was applied for all peptide-level identifications. Only unique and razor peptides were used for quantifiction. Proteins that were detected by at least two peptides were used for quantitative analysis. A mean value of at least four LC-MS/MS replicate quantitative measurements was used in downstream differential, clustering and pathway analysis. For differential expression of proteins, the fold change (FC) was defined as the ratio of replicate averaged normalized LFQ intensities for the test and control case respectively. Log2-ratios for proteins which were quantified in at least 50% of the replicates of test and control respectively, were considered and the log-ratios were median centered to zero. The criterion, abs(log2(FC)) >=1.0 was used to ascertain differentially expressed proteins. The proteomic data set containing Entrez Gene identifiers and fold changes of identified protein was analyzed by the Ingenuity Pathway Analysis (IPA) (Ingenuity Systems, Redwood City, CA). Core analysis with indirect and direct relationships, proteins interactions and pathways, upstream regulatory analysis and functional network identifications were carried out as per manufacturer's instructions using the human database (Qiagen Inc.) [27]. Activation and inhibition of cell functions and upstream regulators were determined according to the Z-score, which is a statistical evaluation of the match between detected protein expression and expected relationship based on literature.

Image acquisition, processing and statistical analysis

Cells were maintained in a humidified stage-top incubator at 37°C and 5% CO_2 and monitored by time-lapse microscopy (Axio Observer.Z1 Microscope (Zeiss, Germany) and Hamamatsu digital camera C10600 Orca-R2) for a total period of 5 hours. Droplets containing calcein AM-labeled target cells and unlabeled NK-92 cells were imaged every 5 minutes with 20x objectives and standard FITC/DAPI/TRITC filters. Specific locations (x-, y-, and z-positions) of droplets containing one effector and one target cell in the droplet docking array were noted in the Zen imaging program (Zeiss) for automated image acquistion. Images were processed with ImageJ

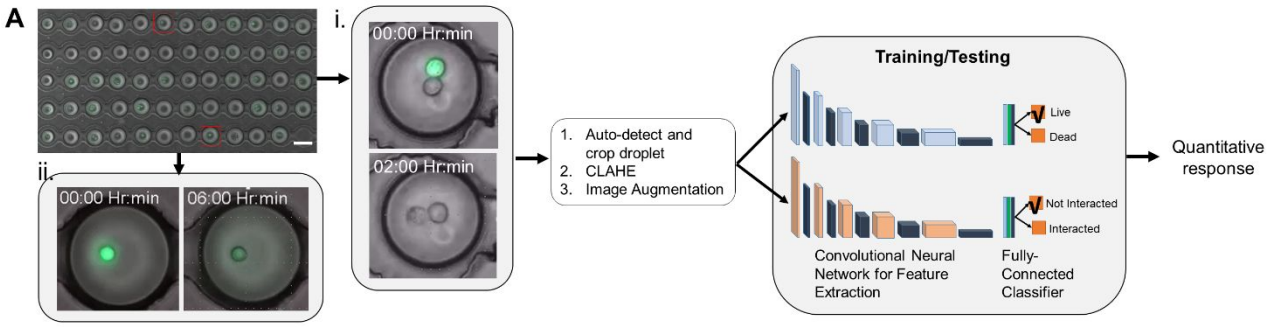

B		Predicted		
		Live	Dead	Accuracy %
Actual	Live	842	38	95.68
	Dead	8	537	98.53

C		Predicted		
		N.I	I	Accuracy %
Actual	N.I	881	59	93.72
	I	33	452	93.19

Fig. 1. Schematic overview of experimental and analytical workflow. (A) Time-lapse images of cell pairs (i) and single cells (ii) in droplet docking array are processed by the machine learning algorithm. Abbreviation: CLAHE- Contrast enhancement using histogram equalization. (B-C) Accuracy of trained analytical program. (B) Confusion matrix of death prediction, containing the number of true positive, true negative, false positive and false negative prediction results. (C) Confusion matrix of interaction prediction.

(**http://rsb.info.nih.gov/ij/**) and quantified with Microsoft Office Excel 2010 and Origin Pro software [8, 9]. Cell death was estimated by ≥80% loss of Calcein AM fluorescence and morphological indicators (e.g., membrane blebbing and rupture) [8, 9, 10]. Contact (stable or intermittent) periods between NK and target cells and frequency were measured per cell pair [8, 9]. All experiments were replicated 2-5 times unless otherwise stated. Statistical analysis was performed using Mann-Whitney U test, and p value <0.05 was considered statistically significant.

NK-92 cells (5×10^4/well) were labeled with a panel of antibodies from Human Cell Surface Marker Screening Panel (BD Biosciences, San Jose, CA) as per manufacturer's recommendation and subjected to laser scanning cytometry. The procedure and imaging parameters are described in Supplementary Methods.

Machine Learning Algorithm

Details of data preprocessing (including contrast enhancement using histogram equalization (CLAHE), image augmentation techniques), convolutional neural network (CNN) and algorithm implementation has been provided in Supplementary Methods.

Results and discussion

Analysis of dynamic interaction parameters with machine learning

We developed a single cell analytical model for determining the dynamics of target cell killing by a two-step process, a droplet microfluidics-based cytotoxicity assay and a machine learning algorithm to identify interactive and viability features (Fig. 1). Effector (NK-92) and target (cancer) cell suspensions were flown through distinct inlets into the T junction of a droplet generator to co-encapsulate heterotypic cell pairs in droplets of 90 ± 10μm diameter [8, 9]. The loaded droplets are docked in the integrated holding array consisting of 4000 locations, enabling dynamic monitoring and analysis of hundreds of E:T cell pairs (Fig. 1A). Droplets containing 0-3 cells of each type were detected in the array due to the stochasticity of trapping procedure. Only droplets containing 1:1 E:T cell ratio were tracked over 5 hours for determining cell-cell interaction and cytolysis (Fig. 1Ai) while droplets containing single NK-92 cell or single target cell were utilized for measurement of spontaneous death (Fig. 1Aii).

Effector lymphocytes interact physically with target cells, forming immunological synapses that allow unidirectional transport of cytotoxic molecules into the target. However, synaptic contact duration varies, and some contacts dissolve without imminent target death. Here, we analyzed the interactions between E:T pairs and NK-mediated cytolysis using a supervised machine learning approach. Images from time-lapse video microscopy were first enhanced with contrast-limited adaptive histogram equalization (CLAHE) algorithm to improve signal to noise ratio and then augmented (i.e., enlargement of the dataset) as described in Supplementary Methods. The images were analyzed with Deep Convolutional Neural Network (CNN) based model; specifically, VGG-19 was used as the backbone network structure to extract meaningful features from the images. VGG network-based approach is commonly used for classification tasks. It contains a number of convolutional layers followed by activation layers and maximum pooling layers. The Rectified Linear Unit (ReLU) function, used as our activation layer, speeded up the training process and ensured that each layer conducted a non-linear operation, essential for CNN function. The extracted features served as input to the Softmax Image classifier to obtain binary classification of death (dead vs live) and interaction (contact vs non-contact). A pilot database of two-channel video files was divided intro training (73 videos) and test (21 videos) sets to train the predictive model to detect interaction between differentially labeled cells and target cell death. We further included a time-related element to the evaluation of death, by implementing a sliding framework of window of size 5, where prediction of death in 3 out of 5 frames would result in the cell being considered dead in all following frames. The accuracy of the algorithm was validated by comparing analytical output side-by-side with manual proofreading. As shown in Fig. 1B,C, the algorithm yielded overall accuracy of >95% and >93% for death and interaction prediction respectively. The high accuracy in interaction and death prediction observed here makes this approach suitable for quantification of pairwise interaction and cytolysis of other therapeutic cell types and high content screening assays.

Parental NK-92 cell-induced death of blood cancer lines in droplets

The developed assay pipeline was then used to test parental NK-92 cell cytotoxicity against hematological cancer lines as NK cells are known to target blood cancer cells efficiently. K562 leukemia cells are frequently used as a target cell line for NK cell cytotoxicity assay [5]. This line was selected for validation of the single cell analytical platform. NK-92 cells significantly ($p < 0.0001$) increased death of K562 compared to spontaneous lysis in droplets (Fig. 2A). NK-92-induced target death occurred at earlier time points (mean: 84 min

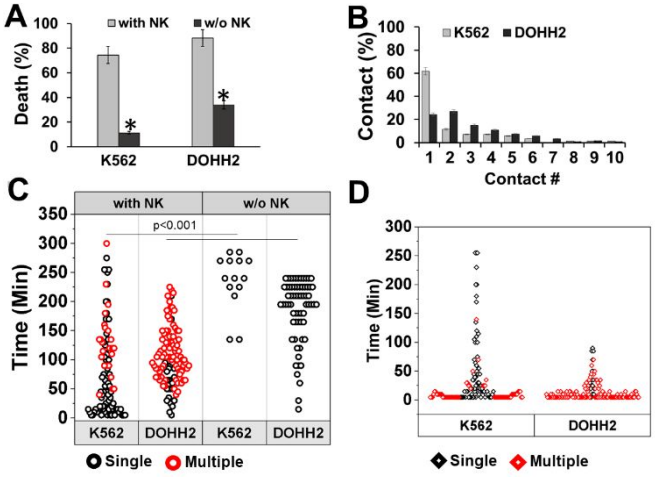

Fig. 2. Interaction of parental NK-92 cells with two hematologic cancer cell lines. (A) Overall death (%) of K562 and DOHH2 cells mediated by NK-92 cells in droplets (with NK: n= 159 and 164 cell pairs respectively, without NK: 168 and 203 respectively). * indicates p<0.001. (B) Contact frequency for K562 and DOHH2 cells. (C) Distribution of death times shown for cell pairs that underwent single and multiple contacts with NK-92 cells. Spontaneous death (i.e., without NK-92 cells) occurs without any contact in droplets containing only target cells. (D) Contact durations between NK-92 and target cells. (C-D) Single contacts are shown by black and multiple contacts by red symbols.

with NK-92 vs 227 min without NK-92, Fig. 2C). 62 ± 3% of K562 died after a single contact with a NK-92 cell (Fig. 2B,C). The duration of single contacts between cell pairs was varied (5-250min, Fig. 2D). A subset of K562 cells dissociated from the conjugates but later interacted with the corresponding NK cell (2-10 contacts, Fig. 2B), and these cells died at later times as evident in Fig 2C. Such multiple contacts usually lasted for shorter periods (5-30min) (Fig. 2D). The correlation coefficient between time of death and conjugation period of cells undergoing single contact with NK-92 cells was high (0.85) while that of multiple contact cells was low (0.23), suggesting a higher likelihood of association between single contact and death (Fig. 2D).

We then tested a lymphoma line DOHH2, which also proved to be susceptible to NK-92-mediated lysis. These cells depicted higher spontaneous lysis in droplets as compared to K562 (34 ± 4% vs 5 ± 1% respectively). But NK-92 cells induced significantly greater and faster DOHH2 death (average death time with and without NK-92 respectively: 103 min and 185 min, $p < .00001$, Fig. 2A,2C). Unlike K562 cells, 75 ± 1 % of DOHH2 cells engaged in multiple contacts with NK-92 cells (Fig. 2B-D). The correlation between contact time and time of death for cells killed following single and multiple contacts ranged from 0.735 to 0.555 respectively. Similar to the K562 line, DOHH2 cell death was significantly delayed in cases of multiple contacts (average death at 56 min for 1 contact vs. 85 min for >1 contact, $p < 0.001$), implying that dissociation of conjugation delayed the onset of cytolysis. These results suggest that cytolysis of the target cells following a single period of conjugation with NK-92 cell occurs more efficiently compared to multiple short associations, as also observed with primary human NK cells [8, 9]. Similar trends have been observed in our previous studies with RPMI-8226 myeloma cells at 1:1 E-T ratio [8]. While NK-92 mediated target death parameters may quantitatively vary depending on the type of platform and analytical process employed, the data trends obtained from the machine learning-based analytical approach are in good agreement with previous studies where interaction and death were measured manually [8, 9].

CD16$^+$/CD16$^-$ NK-92 cells show limited basal cytotoxicity against HER2$^+$ cells

HER2/neu characterizes one of the three major subtypes of breast cancer and has been detected in other gynecological cancers (e.g., ovary, endometrial, cervical) as well as other solid tumors [28]. Although anti-HER2 drugs like trastuzumab (Herceptin) have improved patient prognosis significantly, clinical evidence suggests relapse, de novo and/or acquired drug resistance and eventual metastasis in many patients [29]. NK-92 cell-based immunotherapies can potentiate the effect of drugs against these cancer cells. We determined the cytolysis of two HER2-expressing solid tumor cell lines, SKBR3 breast cancer and SKOV3 ovarian cancer, in droplets (Fig. 3A) [30, 31].

Co-encapsulation of SKBR3 cells with NK-92 cells at 1:1 E:T resulted in 14 ± 1% death of SKBR3 cells compared to 2 ± 1% spontaneous death (Fig. 3B). These target cells made 1-9 contacts in total but 77 ± 4% of the cells made single contact (Fig. 3C); the average duration of single and multiple contacts are shown in Fig. 3D. Despite the lengthy conjugation NK-92 cells demonstrated significantly less lysis of SKBR3 cells compared to K562 and DOHH2.

We also detected very limited death of SKOV3 cells at 1:1 E:T (4 ± 0.1%, Fig. 3B). This was not due to the lack of conjugation between the two cell types, as 86 ± 4% cells made contact in the experimental duration (as also observed in SKBR3 cells) (Fig. 3B). The frequency of contacts was distributed (1-13) (Fig. 3C). As with other cell lines, we observed a marked difference ($p < 0.0001$) between periods of single contacts and multiple contacts (Fig. 3E). The single contacts were either short scanning motions (5 min) or long stable contacts lasting throughout the experimental duration (270 min); multiple contact durations were more varied, but neither type of contacts led to successful target cell cytolysis (Fig. 3E).

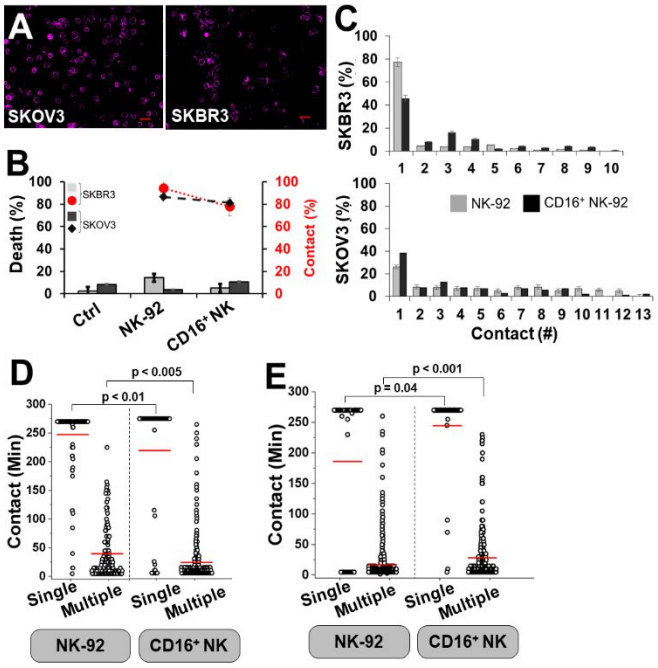

Fig. 3. Interaction of parental and CD16$^+$ NK-92 cells with HER2$^+$ target cells. (A) HER2 expression in SKOV3 and SKBR3 cells. Scale bar: 50 µm. (B) Death (%) of SKBR3 and SKOV3 cells mediated by NK cells (SKBR3: n=141 and 173 cell pairs; SKOV3: n=164 and 128 cell pairs for parental NK-92 and CD16$^+$ NK-92 respectively). Ctrl indicates spontaneous death of SKBR3 and SKOV3 cells in droplets (n=345 and 249 respectively). The extent of contact initiated by NK-target cell pairs are shown on secondary y-axis. (C) Single and multiple contacts made between NK-92-target cell pairs. (D-E) Contact duration occurring between (D) SKBR3 – NK-92 and (E) SKOV3 – NK-92 cell pairs, divided between single contact and multiple (2-10) contacts. Mean of the distribution is indicated in red. Statistical significance values are listed.

Since parental NK-92 cells do not express CD16, they cannot facilitate ADCC. A CD16$^+$ NK-92 cell line has previously been developed to address this limitation. It mediated the death of target cells due to higher Fc affinity and increased levels of Granzyme B secretion [5]. Here we co-encapsulated single CD16$^+$ NK-92 cells with SKBR3 and SKOV3 cells in droplets. In the absence of antibodies CD16$^+$ NK-92 cells minimally altered the death rate of either line (SKBR3: 5 ± 4%; SKOV3: 11 ± 0.5%) (Fig. 3B). However, SKOV3 cells formed significantly longer-lasting conjugates with CD16$^+$ NK-92 cells compared to parental NK-92 cells, both in case of single contact cells and multiple contact cells (p values indicated in Fig. 3E). But this profile was reversed for SKBR3 cells (Fig. 3D), thus depicting cell line-based specificity in interactive features. These results show that NK-92 cells are not cytotoxic at 1:1 E:T towards these HER2$^+$ lines, regardless of CD16 expression, without further stimulation.

Herceptin increases CD16$^+$ NK-92-mediated cytolysis of SKOV3 in a time- and temperature-dependent manner

The CD16$^+$ NK-92 cells have been previously shown to increase cytolysis of various tumor lines via ADCC initiated by the binding of antibodies such as cetuximab with the target cells [5]. Here we tested the ability of CD16$^+$ NK-92 cells to lyse SKOV3 cells pre-treated with 1µg/mL of Herceptin for 30 or 60 min. Since the binding of therapeutic antibodies can depict differential kinetics at varying temperatures [32,33], we decided to assess Herceptin-dependent cytolysis at room temperature (RT) and 37°C (Fig. 4). At 1:1 E:T, addition of Herceptin at RT did not alter the death of SKOV3 cells regardless of the pre-treatment duration (30 min: 12 ± 8%; 60 min: 3 ± 1%, Fig. 4A). Likewise, it did not change the frequency or duration of conjugation (average single contact: 250 min and 227 min for 30 min and 60 min Herceptin pre-treatment respectively) compared to control cells (i.e., no Herceptin) (Fig. 4B). As observed with the parental NK-92 line, E-T pairs that dissociated and made multiple contacts displayed shorter conjugations compared to the long-lasting single contacts (Fig. 4B).

In contrast, conjugating Herceptin with SKOV3 cells at 37°C prior to co-encapsulation with CD16$^+$ NK-92 cells increased death of SKOV3 cells markedly (30 min: 50 ± 16% at 30min, 60 min: 56 ± 11%, Fig. 4A). In case of SKOV3 cells that died following single contacts with NK-92 cells, the interactive durations were significantly shorter (average value: 119 min and 47 min for 30 min and 60 min Herceptin pre-treatment respectively, $p < 0.001$) compared to that at RT or control condition (Fig. 4C). Largely similar trends were obtained for SKOV3-CD16$^+$ NK-92 cell pairs that demonstrated multiple contacts. This decrease in conjugate duration was not due to delayed recognition or disassociation of cell pairs but the fact that SKOV3 cells were killed following interaction with CD16$^+$ NK-92 cells at 37°C, whereas at RT they remained viable despite conjugation. Furthermore, pre-treating SKOV3 cells with Herceptin for 60 min at 37°C resulted in faster cell death and thus shorter conjugation times in comparison with the 30 min pre-treatment, as shown in Fig. 4D.

There is currently little literature on the application of adoptive transfer of NK cell therapies in HER2$^+$ ovarian cancer. EGFR/HER family-targeted therapeutics have been successful in treatment of

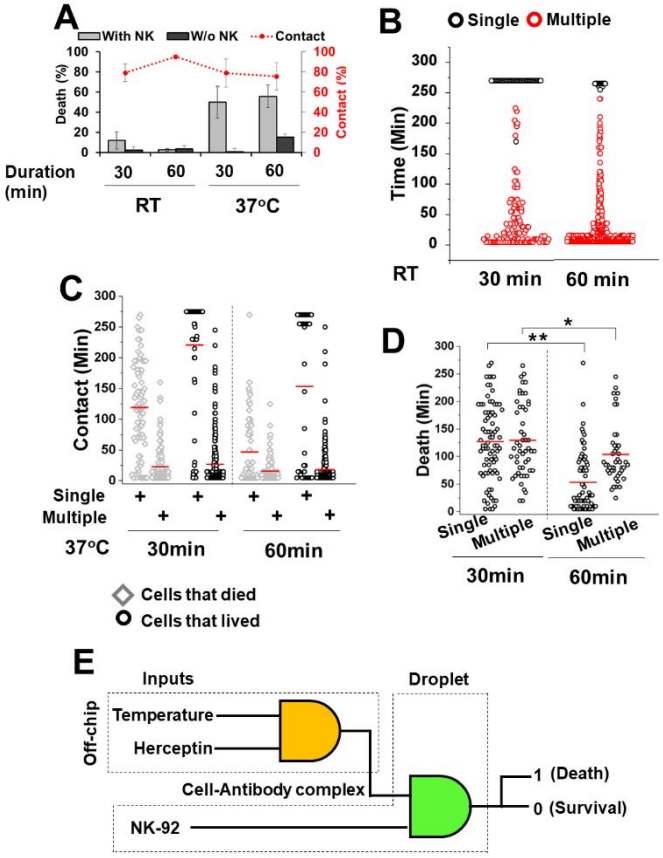

Fig. 4. Interaction between Herceptin-conjugated SKOV3 and CD16$^+$ NK-92 cells. (A) Death (%) of SKOV3 cells mediated by Herceptin (1µg/mL) at different temperature and incubation periods (n=165, 166, 171, 191 cell pairs respectively). The overall % of SKOV3 cells initiating contact with NK cells in droplets is shown in the secondary y-axis in red. (B) Single (black circles) and multiple (red circles) contacts made between SKOV3-NK cell pairs. SKOV3 cells were incubated with Herceptin at room temperature (RT) for 30 or 60 min before encapsulation in droplets. (C) Contact durations made by SKOV3 cells that either died (gray diamonds) or survived (black circles) following interaction with NK cells. SKOV3 cell data was further separated between cells undergoing one or multiple contact with NK cells. The cells were incubated with Herceptin at 37°C for 30 or 60 min before encapsulation in droplets. (D) Time of cell death. * indicates $p<0.05$; ** indicates $p<0.001$. (C-D) Mean of the distribution represented by red lines. (E) Schematic of three-input AND gate function with SKOV3 viability as output.

various solid tumors, so there is a clear basis for testing the combination of Herceptin and the highly cytotoxic NK-92 in HER2+ ovarian cancer. Previous studies have noted that the success of ADCC, that is, death of target cells, relies on pre-incubation of NK cells with the antibody [34,35]. The duration of incubation depended on various factors including the affinity and concentration of the antibody and the density of receptors on the cell surface. Here, the duration of antibody pre-incubation at 37°C also proved to be a significant consideration in mediating faster ADCC in SKOV3 cells. Whether this effect persists in other HER2+ ovarian lines or primary cells remains to be seen. Clinical trials with allogeneic NK cells and cytokine-activated NK cells are still in early phases in ovarian cancer [36]. The results presented here suggest that a combination of CD16+ NK-92 and Herceptin warrant further investigation in *in vitro* and preclinical studies.

Input 1	Input 2	Input 3	Output	
NK-92	Herceptin	Temperature (37°C)	Target Death	Average %
0	0	0	0	-
0	0	1	0	8 (Low)
0	1	0	0	3 (Low)
0	1	1	0	15 (Low)
1	0	0	0	8 (Low)
1	0	1	0	10 (Low)
1	1	0	0	3 (Low)
1	1	1	1	56 (High)

Table 1. Truth table for AND gate function using CD16+ NK-92 cells, Herceptin (1µg/mL, 60 min) and 37°C incubation temperature as inputs and SKOV3 cell death as output.

Summarizing the results of the various incubation conditions, one can postulate that the specific pre-incubation conditions of Herceptin serve as two inputs to control cell-mediated logic operation in droplets (Fig. 4E). Using CD16+ NK-92 cells as the third essential input and SKOV3 death as the output, a truth table for AND logic operation can be constructed (Table 1). A detectable output (=1) is obtained only when all three inputs are positive; in this case, the off-chip Herceptin incubation temperature must be held at 37°C, for 60 min, before co-encapsulating the target cell-antibody complexes with CD16+ NK-92 cells in droplets. In any other condition the SKOV3 cytotoxicity is markedly lower (output = 0). On the other hand, the addition of parental NK-92 cells to K562 targets acts as an inverter, that is, target cells survive in droplets in the absence of NK-92 (input 0) but show an average value of 75 % death in the presence of NK-92 (input 1) (Table 2). The same can be said of DOHH2 cells in droplets. Boolean operations have previously been performed with diverse inputs such as photodynamic therapy agents, DNA, proteins and whole cells [37-40]. Whole cell-based biocomputing has applications in infectious diseases, cancer, metabolic disorders and environmental sensing [38]. The examples of *in vitro* cellular logic gates shown here can potentially be employed in its present condition or in combination with other molecules and drugs as part of a biomolecular computer for immunotherapeutic applications.

Input	Output	
NK-92	K562 Survival	Average %
0	1	88 (High)
1	0	25 (Low)

Table 2. Truth Table for Invert function with K562 cell survival as output.

Effect of Herceptin on SKBR3 cells

CD16+ NK-92 enhanced the death of SKBR3 cells in Herceptin - dependent manner (with/ without Herceptin: 24 ± 2% / 5 ± 4%), although not to the extent observed in SKOV3 cells (Fig. 5A). The contact durations exhibited by CD16+ NK-92-SKBR3 cell pair were similar in the presence and absence of Herceptin in the case of cells that did not undergo cytolysis (Fig. 5B). The target cells that were killed by CD16+ NK-92 cells displayed shorter single contacts compared to cells that survived (132 min vs 197 min respectively, $p < 0.05$), as also detected in SKOV3 cells. The distribution of death times was comparable for death initiated by single and multiple contacts (Fig. 5C).

Although SKBR3 cells express HER2, the moderate increase in killing, along with the finding that the expression of CD16+ in NK-92 cells failed to enhance contact with SKBR3 (Fig. 3D), appears to suggest that further chemical or genetic sensitization strategies will be required to induce SKBR3 death by NK-based immunotherapies. It has been shown previously that Herceptin (trastuzumab) or pertuzumab does not cause a strong inhibition of SKBR3 cell cycle progression, but SKBR3 cells have been shown to express decreased sensitivity to Herceptin compared to other breast cancer lines [32]. SKBR3 cells were not lysed by NK-92 cells despite the lack of HLA class I, which may be essential for NK cell recognition and lysis in cells that express KIRs [41]. Given the long-lasting conjugates formed between NK-92 and a subset of SKBR3, it is also possible that these cells could be lysed after several hours, that is, past the experimental duration of this study. Drugs such as lapatinib or menadione may also facilitate NK-mediated death of these cancer cells [30, 42], but an extensive characterization of stimulants was beyond the scope of this study.

Deep proteomic profiling of NK-92 variants

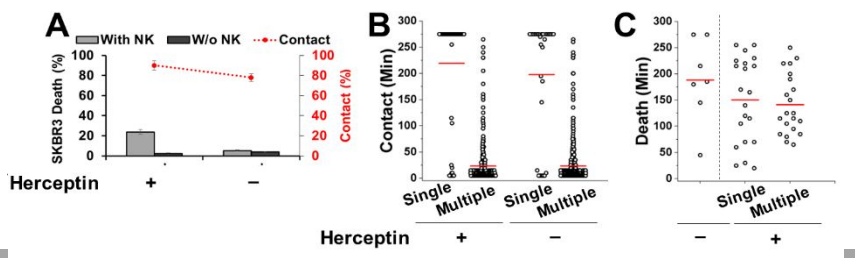

Fig. 5. Interaction between Herceptin-conjugated SKBR3 and CD16+ NK-92 cells. (A) Death (%) of SKBR3 with Herceptin (1µg/mL, at 37°C for 30 min, n=191 cell pairs) and without Herceptin (n=173 cell pairs). The overall % of SKBR3 cells initiating contact with CD16+ NK cells in droplets is shown in the secondary y-axis. (B) Contact profile and (C) death times of SKBR3 cells following incubation with Herceptin. Mean of the distribution is indicated in red.

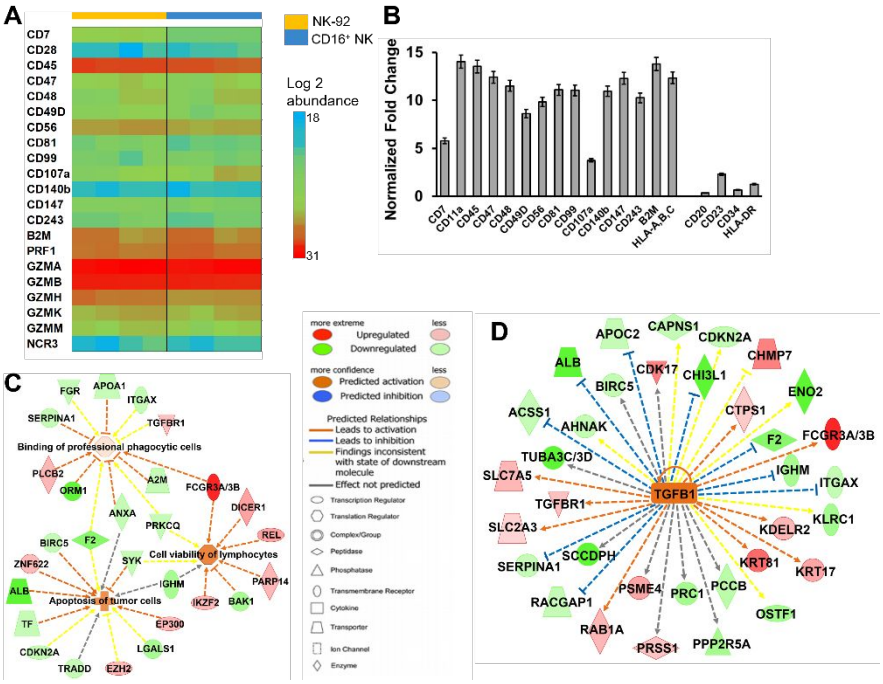

Fig. 6. Selected results of deep proteome profiling of NK cell lines. (A) Examples of proteins quantified by nano LC-MS in parental and CD16$^+$ NK-92 cells. Data obtained from at least n=4 replicates per line. (B) Confirmation of protein expression in parental NK-92 by quantitative laser scanning cytometry. Expression levels have been normalized to IgG control. Data is represented as average ± std. dev. B2M: beta 2 microglobulin. (C) Prediction of activated biological functions in CD16$^+$ NK cells. (D) Identification of TGFβ1 as a key upstream regulator in CD16$^+$ NK -92 cells.

Since the CD16$^+$ and CD16$^-$ NK-92 cells demonstrated differences in cytotoxicity against the target cells in our study, we conducted a comparative proteomic profiling of the two cell types. At least 3571 proteins were identified in each of the cell lines after applying the filtering criteria (FDR ≤ 1%) as described in Materials and Methods (Fig. S1A). Based on the results of hierarchical clustering, the cluster of most abundantly expressed proteins in the NK-92 cell line included cytoskeletal components (actin, myosin, tubulin), histone H1, heat shock protein family members (HSP90, HSPA5) but also granzymes A and B (Fig. S1B) [43]. As expected, expression of other known NK-92 markers such as CD7, CD28, CD56 (NCAM1) and CD107a (LAMP1) were detected in the examined NK-92 lines, as well as MHC class II molecules. Markers associated with cytotoxicity such as natural cytotoxicity receptor (NCR3), perforin and granzymes H, K and M were also detected in both lines (Fig. 6A). The expression levels of a number of proteins detected by mass spectrometry-based proteomic profiling in parental NK-92 were subsequently confirmed by quantitative imaging cytometry (Fig. 6B). NK-92 cells do not express CD20, CD23, CD34 and HLA-DR; these proteins were not detected by imaging cytometry (as shown) or proteomic analysis. Based on pathway enrichment analysis by IPA, intracellular pathway-associated proteins belonging to mTOR, EGFR, VEGF, PI3K/AKT, GMCSF and IL12 signaling pathways were detected in the NK cells; notably, mTOR signaling was found to be one of the top five canonical pathways (Fig. S2). Proteins related to cell functions such as oxidative phosphorylation were detected strongly, as was the oxidative stress response and reactive oxygen species (ROS) production pathways. The phagocytic capability of NK cells was also noted due to the expression of proteins such as LAMP1/2, VAMP2/3, a number of cathepsins (A, C, D, S), V-type proton ATPase subunits, ezrin, Rac and Vav among others.

Comparing the abundance levels of proteins in CD16$^+$ NK-92 cells with the parental NK-92 cells, 249 candidates were found differentially altered in CD16$^+$ NK-92 cells (absolute value of log 2 ratio > 1). Pathway enrichment analysis revealed that the detected candidates were involved in key cellular processes such as IL12 signaling, clathrin mediated endocytosis, metabolism, transport and protein localization. As expected, FCGR3 (CD16) was upregulated in this line, which led to the prediction of increased binding, increased cell viability and decreased apoptotic potential (Fig. 6C). However, in the absence of target cells or engagement by activating ligands the degranulation pathway was not activated. NK cells appear to kill targets rapidly by using granzyme B and slowly by other death receptor pathways [44]. Given that CD16$^+$ NK-92 cells showed high granzyme expression in our study as well as previous studies [5], we checked the expression of candidate proteins known to be associated with granzyme B in NK cell cytotoxicity. Molecules such as SERPINA1 and STXBP1, known to cause degranulation and exocytosis in neutrophils and platelets, were detected in the CD16$^+$ NK-92 cells (Fig. 6C). SERPINA1 inhibits granzyme in human cells [45]; downregulation of this molecule in CD16$^+$ NK-92 could suggest increased availability of granzyme in this line and bears further investigation. Likewise, upregulation of the Rel subunit of NF-κB (Fig. 6C) could also suggest a potential link with enhanced cytotoxicity as the NF-κB pathway regulates granzyme B in NK cells [46]. Pathway analysis identified TGFβ1 as a key regulator of CD16$^+$ NK-92 cells specifically due to the altered expression of a number of molecules of this pathway (Fig. 6D). This is in line with literature reports that have shown that TGFβ inhibits NK-mediated ADCC and CD16-dependent IFN-γ activity [47]. Overall, these proteomic signatures suggest that engineering NK-92 cell lines in different ways has an effect on abundance levels of associated or off-target proteins, which has an impact on critical biomolecular processes.

Mass spectrometry-based profiling of NK-92 cells have been carried out in the past. Although these reports identified relatively small (e.g., 60) groups of proteins, molecules belonging to biosynthesis, transport, metabolism and chaperones were identified [48], just as in our study. Another study characterized proteins regulated by

interferon-alpha (IFN-alpha) and interleukin-15 (IL-15) as these cytokines are known to activate NK cells [49]. Our study was able to detect larger panel of proteins, including candidates belonging to IL-15 and IL-8 pathway, in line with the previous reports. ERK1/2 and Akt kinase (Akt) pathways have been known to be activated by IL2 stimulation, which is required for NK-92 survival and proliferation [44]. The mTOR pathway, one of the top canonical pathways detected here, is also postulated to be critical for the development and activation of NK cells [50,51]. No other study has done a deep proteomic profiling of $CD16^+$ NK-92, which revealed some off-target differences with respect to the parental line. Of note, the prediction of TGFβ as a master regulator has important consequences in cancer immunotherapy as this is a highly immunosuppressive cytokine found in the tumor microenvironment. Potentially, our finding suggests that $CD16^+$ NK-92 may require desensitization to TGFβ during activation to overcome the possibility of immunosuppression[52].

Conclusions

The combination of microfluidic droplet generation/docking platform and machine learning algorithm provided detailed quantification of the dynamic functional parameters of the NK-92 line against NK-sensitive hematologic cancer cells and NK-tolerant $HER2^+$ cancer cells. Although two $HER2^+$ lines were tested at 1:1 E-T in droplets, the combination of Herceptin and $CD16^+$ NK-92 was more effective in enhancing contact and cytotoxicity against SKOV3 cells. The quantitative features detected in the functional assay, such as enhanced cell adhesion, were matched by the findings of the proteomic analysis. In future, incorporating more phenotypic features in the deep learning-based analytical software and automating live cell imaging will allow us to develop a faster, more robust diagnostic and predictive toolbox. We anticipate validating this analytical approach in other cell types and in the presence of immunogenic therapies, which could lead to valuable insights into the role of effector cell-based vaccines and facilitate prediction of therapeutic efficacy in clinical treatments.

Conflicts of interest

There are no conflicts to declare.

Acknowledgements

The authors are grateful for the support provided by NIH/NCI grants (1R33CA223908-01 and 1R01GM127714-01A1) awarded to T.K. A.R.I. acknowledges support by the NIH awards 1R01GM120272 and R01CA218500. The authors would like to thank Dr. Antonius Koller for his assistance with the proteomic experiments.

Author contributions

S.S. and W.K. designed the experimental setup with assistance from T.K., S.S., and W.K. conducted all microfluidic experiments and analyzed the data. S.J. and K.L. designed the machine learning algorithm under the supervision of Y.F. E.L. performed imaging cytometry and data analysis. S.R. analyzed proteomic experiments. S.S. wrote the paper. Y.F., A.R.I. and T.K. supervised the work and provided technical leadership. All co-authors contributed to the paper with critical comments and suggestions.

References

1 S. Srivastava and S.R. Riddell SR, *J Immunol*., 2018, **200**, 459-468.
2 S.A. Rosenberg and N.P. Restifo, *Science*. 2015, **348**, 62.
3 H. Klingemann, *Oncoimmunology*, 2014, **3**, e28147.
4 H. Klingemann, L. Boissel, and F. Toneguzzo, *Front Immunol*. 2016, 7, 91.
5 C. Jochems, J.W. Hodge, M. Fantini, R. Fujii, Y.M. Morillon 2nd, J.W. Greiner, M.R. Padget, S.R. Tritsch, K.Y. Tsang, K.S. Campbell, H. Klingemann, L. Boissel, S. Rabizadeh, P. Soon-Shiong, and J. Schlom, *Oncotarget*, 2016, **7**, 86359.
6 C. Zhang, P. Oberoi, S. Oelsner, A. Waldmann, A. Lindner, T. Tonn, and W.S. Wels, *Front Immunol.*, 2017, **8**, 533.
7 J.S. Orange, *Nat Rev Immunol*., **2008**, 8, 713.
8 S. Sarkar, S. McKenney, P. Sabhachandani, J. Adler, X. Hu, D. Stroopinksy, J. Rosenblatt, D. Avigan, and T. Konry, *Sens Actuators B Chem*., 2019, **282**, 580.
9 S. Sarkar, P. Sabhachandani, D. Ravi, S. Potdar S. Purvey, A. Beheshti, A.M. Evens, and T. Konry, *Front Immunol*., 2017, **8**, 1736.
10 B. Vanherberghen, P.E. Olofsson, E. Forslund, M. Sternberg-Simon, M.A. Khorshidi, S. Pacouret, K. Guldevall, M. Enqvist, K.J. Malmberg, R. Mehr, and B. Önfelt, *Blood*, 2013, **121**, 1326.
11 S. Varchetta, N. Gibelli, B. Oliviero, E. Nardini, R. Gennari, G. Gatti, L.S. Silva, L. Villani, E. Tagliabue, S. Ménard, A. Costa, F.F. Fagnoni, *Cancer Res*., 2007, **67**, 11991.
12 W. Wang, A.K. Erbe, J.A. Hank, Z.S. Morris, P.M. Sondel, *Front Immunol*. ,2015, **6**, 368.
13 C. Jochems, J.W. Hodge, M. Fantini, K.Y. Tsang, A.J. Vandeveer, J.L. Gulley, and J. Schlom J, *Int J Cancer*., 2017, **141**, 583.
14. A.A. Stepanenko and H.H. Heng. *Mutat Res*., 2017, **773**, 91.
15 C. Scheeder, F. Heigwer, and M. Boutros, *Curr Opin Syst Biol*., 2018, **10**, 43.
16 J.B. Lugagne, S. Jain, P. Ivanovitch, Z. Ben Meriem, C. Vulin, C. Fracassi, G. Batt, and P. Hersen, *Sci Rep*., 2018, **8**, 11455.
17 S. Robinson, L. Guyon, J. Nevalainen, M. Toriseva, M. Åkerfelt, and M. Nees, *PLoS One*., 2015, **10**, e0143798.
18 O.Z. Kraus, B.T. Grys, J. Ba, Y. Chong, B.J. Frey, C. Boone, and B.J. Andrews, *Mol Syst Biol*., 2017, **13**, 924.
19 M.S. Manak, J.S. Varsanik, B.J. Hogan, M.J. Whitfield, W.R. Su, N. Joshi, N. Steinke, A. Min, D. Berger, R.J. Saphirstein, G. Dixit, T. Meyyappan, H.M. Chu, K.B. Knopf, D.M. Albala, G.R. Sant, and A.C. Chander, *Nat Biomed Eng*. 2018, **2**, 761.
20 F. Fuchs, G. Pau, D. Kranz, O. Sklyar, C. Budjan, S. Steinbrink, T. Horn, A. Pedal, W. Huber, and M. Boutros, *Mol Syst Biol*., 2010, **6**,370.
21 W.J. Godinez, I. Hossain, S.E. Lazic, J.W. Davies, and X. Zhang, *Bioinformatics*., 2017, **33**, 2010.
22 B. Dura, M.M. Servos, R.M. Barry, H.L. Ploegh, S.K. Dougan, and J. Voldman, *Proc Natl Acad Sci* U S A., 2016, **113**, E3599-E35608.
23 M. Abonnenc, M. Borgatti, E. Fabbri, R. Gavioli, C. Fortini, F. Destro, L. Altomare, N. Manaresi, G. Medoro, A. Romani, M.

Tartagni, E. Lo Monaco, P. Giacomini, R. Guerrieri, and R. Gambari, *J Immunol*., 2013, **191**, 3545-3552.
24 C. Uherek, T. Tonn, B. Uherek, S. Becker, B. Schnierle, H.G. Klingemann, and W. Wels, *Blood*. 2002, **100**, 1265.
25 S. Sarkar, N. Cohen, P. Sabhachandani, and T. Konry, *Lab C*hip. 2015, **15**, 4441.
26 S. Sarkar, P. Sabhachandani, D. Stroopinsky, K. Palmer, N. Cohen, J. Rosenblatt, D. Avigan, and T. Konry, *Biomicrofluidics*, 2016, **10**, 054115.
27 A. Krämer, J .Green, J. Pollard Jr, and S. Tugendreich, *Bioinformatics*, 2014, 30, 523-530.
28 N.M. Ayoub, K.M. Al-Shami, and R.J. Yaghan, *Breast Cancer (Dove Med Press)*. 2019, **11**, 53.
29 P.R. Pohlmann, I.A. Mayer, and R. Mernaugh, *Clin Cancer Res*., 2009, **15**, 7479-7491.
30 S. Diermeier-Daucher, S. Breindl, S. Buchholz, O. Ortmann, and G. Brockhoff, *Cytometry A*, 2011, **79**, 684.
31 A. Magnifico, L. Albano, S. Campaner, D. Delia, F. Castiglioni, P. Gasparini, G. Sozzi, E. Fontanella, S. Menard, and E. Tagliabue, *Clin Cancer Res.,* 2009, **15**, 2010.
32 R.W. Johnstone, S.M. Andrew, M.P. Hogarth, G.A. Pietersz, and I.F. McKenzie, *Mol Immunol.,* 1990, **27**, 327.
33 J.C. Encarnação, P. Barta, T. Fornstedt, and K. Andersson, *Biomed Rep*., 2017, **7**, 400.
34 G. Romain, V. Senyukov, N. Rey-Villamizar, A. Merouane, W. Kelton, I. Liadi, A. Mahendra, W. Charab, G. Georgiou, B. Roysam, D.A. Lee, and N. Varadarajan, *Blood*., 2014, **124**, 3241.
35 Y. Tang, J. Lou, R.K. Alpaugh, M.K. Robinson, J.D. Marks, and L.M. Weiner, *J Immunol*., 2007, **179**, 2815.
36 S. Nersesian, H. Glazebrook, J. Toulany, S.R. Grantham, and J.E. Boudreau, *Front Immunol*., 2019, **10**, 1782.
37 S. Erbas-Cakmak, S. Kolemen, A.C. Sedgwick, T. Gunnlaugsson, T.D. James, J. Yoon, and E.U. Akkaya. *Chem Soc Rev*., 2018, **47**, 2228-2248.
38 M. You, G. Zhu, T. Chen, M.J. Donovan, W. Tan, *J Am Chem Soc*., 2015, **137**, 667-674.
39 K.Y. Tomizaki, and H. Mihara, *J Am Chem Soc*., 2007, **129**, 8345-8352.
40 B. Saltepe, E.S. Kehribar, S.S. Su Yirmibeşoğlu, and U.Ö. Şafak Şeker. *ACS Sens*., 2018, 3, 13-26.
41 E. Mamessier, A. Sylvain, F. Bertucci, R. Castellano, P. Finetti, G. Houvenaeghel, E. Charaffe-Jaufret, D. Birnbaum, A. Moretta, D. Olive, *Cancer Res*., **2011**, 71, 6621.
42 S. Sajadimajd, R. Yazdanparast, *Mol Cell Biochem*., **2015**, 408, 89.
43 D. Szklarczyk, A.L. Gable, D. Lyon, A. Junge, S. Wyder, J. Huerta-Cepas, M. Simonovic, N.T. Doncheva, J.H. Morris, P. Bork, L.J. Jensen, and C.V. Mering. *Nucleic Acids Res*., 2019, **47**, D607-D613.
44 I. Prager, C. Liesche, H. van Ooijen, D. Urlaub, Q. Verron, N. Sandström, F. Fasbender, M. Claus, R. Eils, J. Beaudouin, B. Önfelt, and C. Watzl, *J Exp Med*. 2019, **216**, 2113.
45 D. Kaiserman, and P.I. Bird, *Cell Death Differ*., 2010, **17**, 586.
46 C. Huang, E. Bi, Y. Hu, W. Deng, Z. Tian, C. Dong, Y. Hu, and B. Sun, *J Immunol*. 2006, **176**, 4173.
47 R. Trotta, J. Dal Col, J. Yu, D. Ciarlariello, B. Thomas, X. Zhang, J. Allard 2nd, M. Wei, H. Mao, J.C. Byrd, D. Perrotti, and M.A. Caligiuri, *J Immunol*. 2008, **181**, 3784.
48. X.C Liu, H. Liang, Z. Tian, Y.S. Ruan, L. Zhang, and Yang Chen, *Biochemistry (Mosc)*., 2007, **72**, 716-727.
49 R. Rakkola, S. Matikainen, and T.A. Nyman, *J. Proteome Res*., 2005, **4**, 1, 75-82.
50 K. Kawauchi, K. Ihjima, and O. Yamada, *J Immunol.,* 2005,**174**, 5261-5269.
51 A.K. Ali, N. Nandagopal, and S.H. Lee, *Front. Immunol*., 2015, **6**, 355.
52 J.A. Foltz, J.E. Moseman, A. Thakkar,1 N. Chakravarti, and D.A. Lee, *Cancers (Basel)*. 2018, **10**, 423.

Table of contents

Comparative proteomic profiling and development of convolution neural network algorithm for quantifying discrete target interaction by engineered NK cells in microfluidic droplets